ISSN: 2688-8645

Dynamic Analysis of a Horizontal Well Drillstring System

Pan Fang [1,*], Ao Shen [1], Chuan Yang [2], Yongchun Wu [2], Caijun Yu [2], Qing Yu [2]

[1] School of Mechanical Engineering, Southwest Petroleum University, Chengdu Sichuan, 610500, China

[2] Downhole Operation Company, CCDC, Chengdu, Sichuan, 610052, China

* Corresponding author: Pan Fang

Abstract

Purpose To address the issue that current dynamic models of drill strings typically simplify the mathematical modeling of the interaction between the drill bit and the rock, thus failing to accurately reflect the actual behavior of the drill bit, this study aims to investigate the dynamic behavior of the horizontal well drill string system equipped with a cone bit under different drilling parameters. Methods In this work, a dynamic mathematical model of the coupled nonlinear system of drillstring-cone bit-rock under the wellbore trajectory of a three-dimensional curved well is established. The drillstring is spatially discretized into multiple Euler–Bernoulli beam elements using the finite element method. The cone bit model is established, which fully accounts for state-dependent delay effects, and multiple cutters interactions. The interaction forces between the bit and the rock were introduced as boundary conditions for the drillstring model, while the displacement of the drillstring's terminal node is used as an input to the bit model, achieving a nonlinear coupling between the bit and the drillstring. The coupled nonlinear dynamic system is solved using the Newmark method combined with an improved Newton–Raphson iteration scheme. Results The numerical results indicate that increasing the rotational speed and the weight on bit (WOB) will intensify the vibration of the drill string, but it will improve the drilling efficiency. A higher rotational speed helps to suppress the sliding vibration of stuck pipe, while a larger WOB can effectively alleviate the axial stuck pipe sliding phenomenon. An increase in the local curvature of the wellbore trajectory will lead to an increase in the vibration intensity of the drill string at that location. An increase in the strength of the formation rock will cause an increase in the vibration intensity of the drill bit and a greater increase in the axial strength than the torsional strength. Conclusion These findings establish a solid theoretical foundation for controlling drillstring vibrations and offer guidance for optimizing drilling parameters and designing suitable bottom-hole assembly configurations.

Keywords

Nonlinear Dynamics; Stick-slip; Bit-bounce; Cone Bit; Drillstring.

1. Introduction

Drilling engineering is fundamental to oil and gas exploration and development, and its expenditures typically account for approximately 50% to 80% of the total project cost. Therefore, improving drilling efficiency is an effective way to reduce overall expenses and enhance economic performance in hydrocarbon production.As illustrated in Figure 1, a conventional drilling system consists of surface facilities and a downhole drillstring assembly. The downhole drillstring is mainly composed of drill pipes and the bottom-hole assembly (BHA), which includes the bit, drill collars, and various auxiliary drilling tools[1][2]. During

ISSN: 2688-8645

rotary drilling operations, the winch and rotary drive system are responsible for hoisting, lowering, and rotating the drillstring. By transmitting weight on bit (WOB) and torque to the drill bit, the BHA enables rock fragmentation and progressive well deepening.Throughout the drilling process, the drillstring is subjected to axial, torsional, and lateral vibrations. These dynamic responses are primarily induced by bending deformation under combined WOB and torque, nonlinear frictional contact and impact between the drillstring and the borehole wall, as well as the complex nonlinear interaction between the bit and the formation. Under such complicated downhole conditions, different vibration modes may develop, including lateral whirl, torsional stick–slip, and axial bit bounce. These vibration modes can occur individually or in coupled forms [3], and they significantly threaten drilling tool integrity, shorten equipment service life, increase operational time and cost, and are recognized as major contributors to drillstring and bit failures. Consequently, to mitigate vibration-related damage and reduce drilling expenditures, it is essential to investigate the underlying mechanisms of vibration and optimize drilling parameters accordingly [4][6].

Many scholars have established numerous mature theoretical models for the study of drillstring dynamics. Early research primarily focused on single-mode vibrations. For example, Han[7] used an infinitesimal linear analysis method to separately analyze the axial, lateral, and torsional vibrations of the drillstring, revealing that vibration frequencies fluctuate with well depth. Li Zifeng[8] established classical differential equations and used difference method, weighted residual method and finite element method to analyze the longitudinal, lateral and torsional vibrations of the drillstring. Similarly, Ren[9], Meng[10], and Fan[11]also contributed to the study of single-mode drillstring vibrations from various perspectives. However, the anisotropic vibrations of the drillstring do not exist independently, people's research gradually deepened to the study of complex coupled vibrations. The simplicity of the lumped mass method makes it appealing to many researchers. Gupta et al.[12] developed an axial–torsional coupled model of the drillstring using the lumped mass method and introduced the rock surface cutting profile to describe the regenerative cutting effect. Their bifurcation analysis revealed a supercritical Hopf bifurcation mechanism responsible for bit bounce and stick–slip vibrations. However, the model focused only on two-dimensional coupling and adopted a simplified bit–rock interaction. Yigit[13] established an axial–torsional lumped parameter model with a motor-driven top boundary and a non-delayed bit–rock interaction at the bottom to describe bit bounce and stick–slip motion. Although the model is simple and computationally efficient, it neglects the time-delay effect in the bit penetration process. Their results showed that bit speed and rock stiffness are the main factors affecting system dynamics, and changing the rotary speed alone cannot eliminate both stick–slip and bit bounce. With the introduction of the finite element method, the lumped mass approach has gradually been replaced due to its limited accuracy and inability to represent complex downhole conditions. Wang et al.[14] used the finite element method to establish a dynamic model of the horizontal well drillstring system. The results showed that the fluctuation of the bit angular velocity was positively correlated with the driving angular velocity, but the study focused only on torsional responses of the bit. Cai et al.[15]also used the finite element method to spatially discretize the drill string in curved wells and proposed a nonlinear dynamic model considering axial–lateral–torsional coupling. The Generalized-α method was employed to obtain the lateral dynamic response of the system. However, Cai only analyzed the influence of drillstring length, driving angular velocity, drill pressure, friction coefficient and stabilizer on the lateral vibration of the drillstring, without studying the axial and torsional vibrations of the drillstring, and ignored the interaction between the bit and the rock. In addition,

Although the application of finite element methods in the study of drillstring dynamics is relatively mature, most existing models employ oversimplified boundary conditions at the drillstring bottom—namely, the bit–rock interaction. In many cases, empirical equations for

ISSN: 2688-8645

Wob and torque are used to approximate bit–rock contact, which does not accurately reflect real downhole conditions. Tobias [16] introduced the regenerative cutting theory, which posits that the surface left by the previous cut influences the depth of the current cut, thereby affecting the variation in cutting forces. This theory has been widely applied in turning, milling, and drilling processes [17]-[19]. E. Detournay [20]developed a PDC bit–rock interaction model that is independent of bit rotation speed. He analyzed the mechanics of a single cutters during cutting and decomposed both the bit torque and WOB into two components: one associated with cutting on the cutters face and the other with friction on the wear flat. A set of force calculation equations was derived accordingly. In recent years, researchers have begun incorporating this aspect into bit–rock interaction modeling. For instance, in 2020, Tian [21] developed a PDC bit–rock interaction model based on the SDD framework using projection principles and polygon clipping techniques. This model effectively captured the cutters layout and geometry, and analyzed how bit design parameters influence system stability. However, the drillstring model in Tian's work was limited to two degrees of freedom and did not explore how the bit model affects the dynamic behavior of the drillstring system.

In summary, there are still several deficiencies in the mathematical modeling of the bit–rock interaction when establishing a drillstring dynamic model. Specifically, the bit model does not reflect the geometric parameters of the bit, the bit model is not coupled with the drillstring model, and the degrees of freedom of the drillstring system are not fully considered. To address these shortcomings, the main contributions of this study are as follows:(1) A bit–rock interaction model is developed that explicitly accounts for the bit cutter layout and geometric parameters. (2) The loading method of the hook load (top boundary of the drillstring system) is optimized to better reflect the actual motion of the drillstring. (4) Appropriate drilling parameters are recommended for common operating conditions.

This study aims to establish a drillstring dynamic model that better reflects real drilling conditions, thereby providing theoretical support for the optimization of drilling parameters.

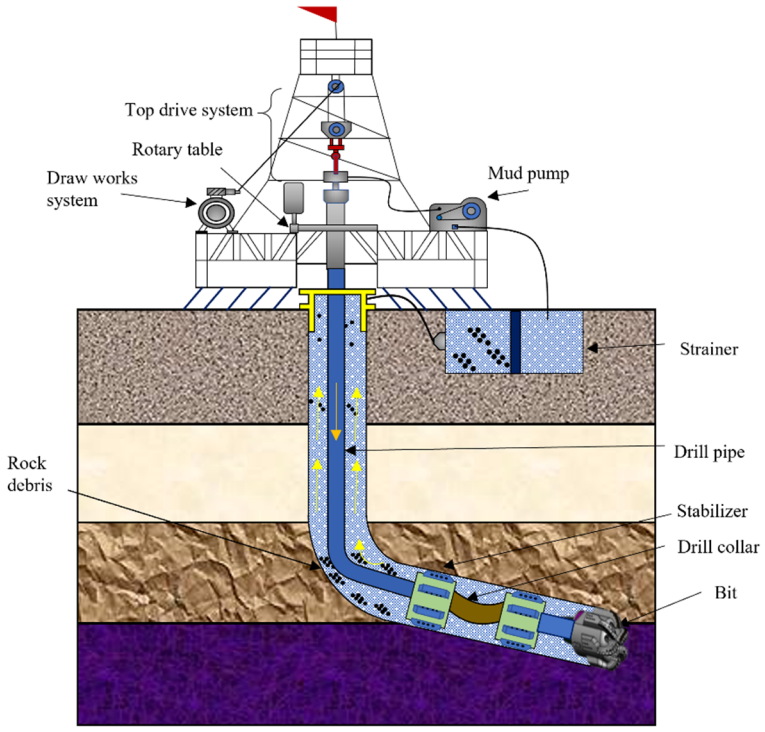

Fig 1. Drilling Column System Model

ISSN: 2688-8645

2. Drillstring Finite Element Dynamic Model

2.1. Coordinate System Establishment

In this paper, three coordinate systems are established: the global coordinate system, the borehole coordinate system, and the local coordinate system to describe the coordinates, deformation, and movement of the drillstring in three-dimensional space. The coordinate establishment is shown in Figure 2. The global coordinate system (*OXYZ*) starts from the wellhead *O*, with north as the *X*-axis, east as the *Y*-axis, and the direction of gravity as the *Z*-axis. The borehle coordinate system (O_1xyz) takes the tangential direction of the wellbore axis as the *x*-axis, the *y*-axis is perpendicular to the *x*-axis pointing to the higher side of the wellbore, and the *z*-axis is determined by the right-hand rule. The local coordinate system ($O_2x_1y_1z_1$) takes the tangential line of the drillstring axis as the x_1 axis, and the determination method of the y_1 and z_1 axes is the same as that of the wellbore coordinate system *y* and *z* axes

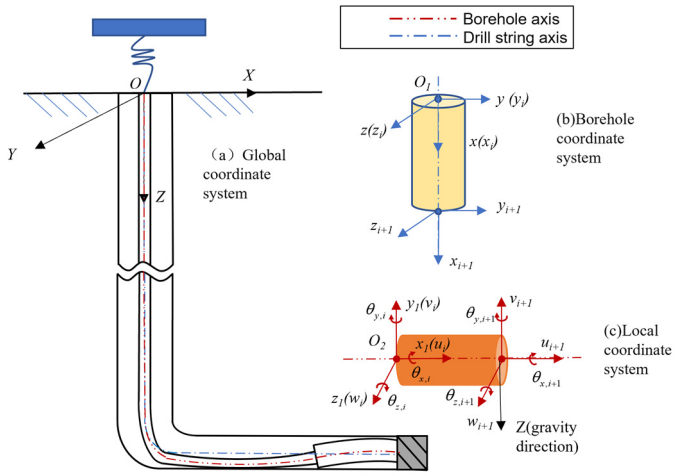

Fig 2. The drillstring coordinate system:(a) Global coordinate system (b) Borehole coordinate system (c) Local coordinate system

2.2. Dynamic Model

The control equation of the drillstring system in local coordinates can be derived through the Lagrange equation. Then, the dynamic response equation of the drillstring system is:

$$\frac{d}{dt}\left[\frac{\partial(T_e - V_e)}{\partial \dot{\mathbf{q}}_e}\right] - \frac{\partial(T_e - V_e)}{\partial \mathbf{q}_e} = \mathbf{F}_e \tag{1}$$

where, T_e is the kinetic energy of the beam element; V_e represents the potential energy of the beam element; $\mathbf{F}_e$ represents the external force applied to the node, $\mathbf{q}_e$ is the displacement of the beam element, and $\dot{q}_e$ represents the derivative of the displacement with respect to time

The total kinetic energy of the beam element includes translational kinetic energy and rotational kinetic energy, and its expression is:

$$\begin{aligned} T_e = {} & \frac{\rho A}{2}\int_0^{l_e}\left(\dot{u}^2 + \dot{v}^2 + \dot{w}^2\right)dx + \frac{\rho}{2}\int_0^{l_e} I_p\dot{\theta}_x^2 dx + \frac{\rho}{2}\int_0^{l_e} I_{yz}(\dot{\theta}_y^2 + \dot{\theta}_z^2)dx + \rho I_p \Omega_{rt}\int_0^{l_e}\dot{\theta}_y\theta_z dx \\ & + \rho A e\Omega\int_0^{l_e}(\dot{w}\cos\beta - \dot{v}\sin\beta)dx + \rho I_p\int_0^{l_e}\Omega_{rt}\dot{\theta}_x dx + \rho I_p l_e\Omega_{rt}^2 \end{aligned} \tag{2}$$

where, $\dot{u}$, $\dot{v}$, and $\dot{w}$ respectively represent the translational velocities of the beam element along the *x*-axis, *y*-axis, and *z*-axis, m/s; θ_x, $\theta_y$and θ_z are respectively the rotation angles of the beam element around the *x*-axis, *y*-axis, and *z*-axis, rad; $\dot{\theta}_x$, $\dot{\theta}_y$ and $\dot{\theta}_z$ are respectively the rotational angular velocities of the beam element around the *x*-axis, *y*-axis, and *z*-axis, rad/s; ρ is the density of the beam element, kg/m^3; l_e represents the length of the beam element, m; A

ISSN: 2688-8645

is the cross-sectional area of the beam unit, m²; I_p is the polar moment of inertia of the cross-section of the beam element, with the element of m⁴. $I_{xy}$is the moment of inertia of the cross-section of the beam element, m⁴. e is the offset caused by the center of mass of the beam element and the rotation center of the beam, m; Ω_{rt} is the wellhead drive speed, rad/s; Ω is the actual rotating speed underground, rad/s; β is the angular position of the center of mass, rad.

The total potential energy expression of the beam element is:

$$V_e = \frac{EA}{2}\int_0^{l_e}\left(\frac{\partial u}{\partial x}\right)^2 dx + \frac{GI_p}{2}\int_0^{l_e}\left(\frac{\partial \theta_x}{\partial x}\right)^2 dx + \frac{EI_{yz}}{2}\int_0^{l_e}\left[\left(\frac{\partial \theta_y}{\partial x}\right)^2 + \left(\frac{\partial \theta_z}{\partial x}\right)^2\right] dx + \frac{EA}{2}\int_0^{l_e}\left(\frac{\partial u}{\partial x}\right)^3 dx$$
$$+ \frac{EA}{2}\int_0^{l_e}\left[\frac{\partial u}{\partial x}\left((\theta_y)^2 + (\theta_z)^2\right)\right] dx + \frac{3EI_{yz}}{2}\int_0^{l_e}\frac{\partial u}{\partial x}\left[\left(\frac{\partial \theta_y}{\partial x}\right)^2 + \left(\frac{\partial \theta_z}{\partial x}\right)^2\right] dx \tag{3}$$
$$+ \frac{EI_p}{2}\int_0^{l_e}\frac{\partial u}{\partial x}\left(\frac{\partial \theta_x}{\partial x}\right)^2 dx + \frac{(E-G)I_p}{2}\int_0^{l_e}\frac{\partial \theta_x}{\partial x}\left(\theta_y\frac{\partial \theta_z}{\partial x} - \theta_z\frac{\partial \theta_y}{\partial x}\right) dx$$

where, E represents the elastic modulus of the beam element, pa; G is the shear modulus of the beam element, pa.

2.3. External Force Model

2.3.1. Gravity, Buoyancy, Unbalanced Force

In Equation (1), F_e is the external force acting on the system. Due to the complex underground environment, the composition of F_e is also very complex. Firstly, the distributed forces (gravity, buoyancy and unbalanced forces) related to their own properties can be derived from the principle of virtual work[22] and be equivalent to acting on the element nodes. The equivalent node force expressions of gravity F_{gra}, buoyancy F_{buo} and unbalanced force F_{imb} are:

$$\mathbf{F}_{\text{gra}} = \left[\frac{q_x l_e}{2} \quad \frac{-q_y l_e}{2} \quad 0 \quad 0 \quad 0 \quad \frac{-q_y l_e^2}{12} \quad \frac{q_x l_e}{2} \quad \frac{-q_y l_e}{2} \quad 0 \quad 0 \quad 0 \quad \frac{q_y l_e^2}{12}\right]^T$$
$$F_{\text{buo}} = -F_{\text{gra}}\frac{\rho_f}{\rho} \tag{4}$$
$$\mathbf{F}_{imb} = \left[0 \quad \frac{f_y l_e}{12} \quad \frac{f_z l_e}{12} \quad 0 \quad \frac{-f_z l_e^2}{12} \quad \frac{f_y l_e^2}{12} \quad 0 \quad \frac{f_y l_e}{2} \quad \frac{f_z l_e}{2} \quad 0 \quad \frac{f_z l_e^2}{12} \quad \frac{-f_y l_e^2}{12}\right]^T$$

2.3.2. Model of the contact between the drillstring and the wellbore wall

When the radial displacement of the drillstring exceeds the gap between it and the wellbore, the drillstring will collide with the wellbore wall. The collision node will be subjected to the radial reaction force F_n, the tangential reaction force F_t and the frictional torque T_f. The drillstring-wellbore collision model is established by using the Hertz contact theory [23]-[24] as shown in Figure 3. The expressions of the radial reaction force F_n tangential reaction force F_t and friction torque T_f are:

$$F_n = \begin{cases} k_c\left(r - \dfrac{(d_w - d_e)}{2}\right) & r > \dfrac{(d_w - d_e)}{2} \\ 0 & r \le \dfrac{(d_w - d_e)}{2} \end{cases}$$
$$F_t = \mu(\Omega_{rel})F_n \tag{5}$$
$$T_f = \frac{d_w}{2}F_t$$

where, k_c represents the contact stiffness of the rock, N/m; d_w is the wellbore diameter, m; d_e is the outer diameter length of the drillstring, m; $r = \sqrt{v^2 + w^2}$, representing the radial

ISSN: 2688-8645

displacement of the drillstring, m; $\mu(\Omega_{rel})$ represent the speed-dependent nonlinear equivalent friction coefficient

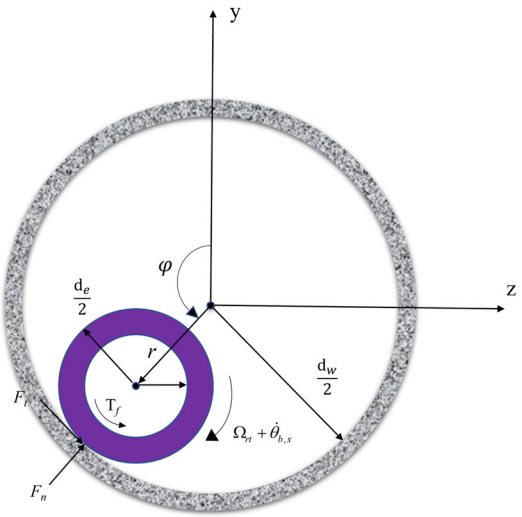

Fig 3. Model of the contact between the drillstring and the well wall

3. Model of the Contact between the Bit and the Rock

As shown in Figure 4, it is the bit-rock interaction model. The instantaneous cutting depth $d_{ij}(t)$ of the cone bit and the torsion angle relationship of the two interacting cutters in the twist direction of the bit are respectively expressed as

$$d_{ij}(t) = u_b(t) - u_b(t - t_{ij}) \tag{6}$$

According to study by Liu Xianbo et al[17], the time delay term t_{ij} is not only related to the previous state of the cutters, but also to the previous N_r states. Therefore, after considering the multiple regenerative cutting effects, the torsional angle relationship of the cutters is expressed as:

$$\Omega_b t_{ij} i + \theta_{i,b}(t) - \theta_{i,b}(t - t_{ij} i) = \Phi_{ij}, \quad j = 1, 2, 3, \ldots, N_r \tag{7}$$

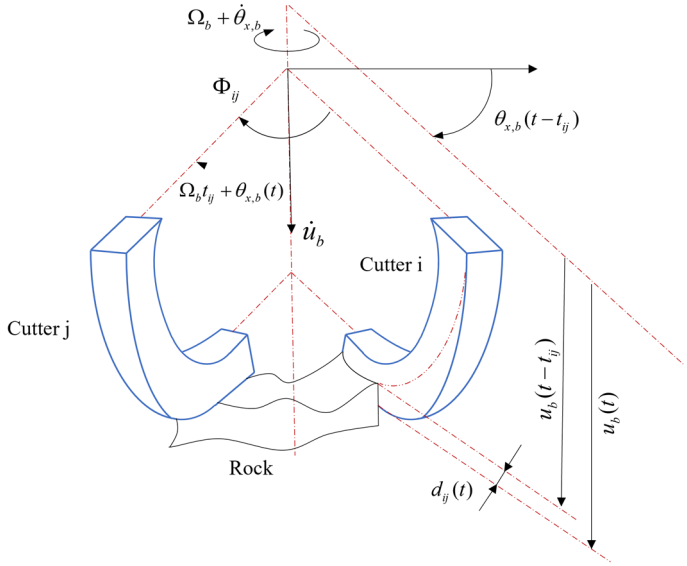

Fig 4. Schematic Diagram of Drill Cutting Depth

where, t represents time, s; t_{ij} represents the time delay of cutters *i* and *j* (the time required for cutter *i* to rotate Φ_{ji} to cutters *j*), s. Equation (7) is an implicit equation related to t_{ij}, indicating

ISSN: 2688-8645

that the time delay term t_{ij} (state-dependent time delay) is not only related to the current state but also to the previous state of the cutters. Solving the equation can yield the time delay t_{ij} at any moment. However, according to study by Liu Xianbo et al[17], the time delay term t_{ij} is not only related to the previous state of the cutters, but also to the previous N_r states.

Therefore, as long as the implicit Equation (7) is solved and the time-delay variable t_{ij} is substituted into equation (6), the cutting depth d_i of the cutter C_i can be obtained:

$$d_i(t) = \min_{i=1}^{N_r}\left(u_b(t) - u_b(t - t_{ij}i)\right) \tag{8}$$

where, ***min(.)***for the minimum value function, after the solution is completed, the cutting depth d_i of all cutters is denoted as the set **D**

Therefore, the weight on bit and torque of the cone bit can be expressed as:

$$W_b(t) = W_{bd} + K_f sin(2\pi n_b f_b t) \tag{9}$$

Where, W_b is the weight on bit (WOB), N; W_{bd} is the average weight on bit, N; K_f is the formation stiffness, N/m; d is the cutting depth of the bit per revolution, in m; n_b denotes the number of blades (for a PDC bit) or the number of cones (for a roller-cone bit); f is the fluctuation frequency of the weight on bit, Hz.

$$T_b(t) = \frac{1}{3} r_h \mu_f W_b(t) = \frac{1}{3} r_h \mu_f [W_{bd} + K_f d \sin(2\pi n_b f_b t)] \tag{10}$$

Where, $T_b(t)$ is the frictional torque acting on the bit at time t, N·m; r_h is the borehole radius, in m; μ_f is the coefficient of dynamic friction between the bit and the borehole wall.

4. Numerical analysis methods

4.1. Numerical Solution of the Dynamic Equations

4.1.1. Newmark Method

the dynamic equation of the unit beam element in the local coordinate system can be expressed as

$$\mathbf{M}_e \ddot{\mathbf{q}}_e + \mathbf{C}_e \dot{\mathbf{q}}_e + \mathbf{K}_e \mathbf{q}_e = \mathbf{F}_e \tag{11}$$

The dynamic model in this paper is solved by using the Newmark method and the improved Newton-Raphson method[25]. The Newmark method can transform the second-order ordinary differential equations of displacement with respect to time into a set of algebraic equations about displacement at discrete time points to obtain approximate solutions. Then, the improved Newton-Raphson method is used to iteratively calculate the approximate solutions at each moment to obtain the exact solutions at that moment.

In the Newmark method, the velocity and displacement at the discrete time point k+1 can be expressed as:

$$\dot{\mathbf{q}}_{k+1} = \dot{\mathbf{q}}_k + [(1-\alpha)\ddot{\mathbf{q}}_k + a\ddot{\mathbf{q}}_{k+1}]\Delta t \tag{12}$$

$$\mathbf{q}_{k+1} = \mathbf{q}_k + \dot{\mathbf{q}}_k \Delta t + \left[\left(\frac{1}{2} - \beta\right)\ddot{\mathbf{q}}_k + \beta \ddot{\mathbf{q}}_{k+1}\right]\Delta t^2 \tag{13}$$

where, α and β are weighting coefficients; k represents the kth time step. Further, from Equations (11) and (11), it can be obtained that:

$$\ddot{\mathbf{q}}_{k+1} = \frac{1}{\beta \Delta t^2}(\mathbf{q}_{k+1} - \mathbf{q}_k) - \frac{1}{\beta \Delta t}\dot{\mathbf{q}}_k - \left(\frac{1}{2\beta} - 1\right)\ddot{\mathbf{q}}_k \tag{14}$$

ISSN: 2688-8645

$$\dot{\mathbf{q}}_{k+1} = \frac{\alpha}{\beta\Delta t}(\mathbf{q}_{k+1} - \mathbf{q}_k) - \left(\frac{\alpha}{\beta} - 1\right)\dot{\mathbf{q}}_k - \left(\frac{1}{2\beta} - 1\right)\ddot{\mathbf{q}}_k \Delta t \tag{15}$$

Substituting equations (14) - (15) into equation (11), the drilling column motion control equation can be expressed using the Newmark method as:

$$(\lambda_1\mathbf{M} + \lambda_4\mathbf{C} + \mathbf{K})\mathbf{q}_{k+1} = \mathbf{F}_{k+1} + M(\lambda_1\mathbf{q}_k + \lambda_2\dot{\mathbf{q}}_k + \lambda_3\ddot{\mathbf{q}}_k) + \mathbf{C}(\lambda_4\mathbf{q}_k + \lambda_5\dot{\mathbf{q}}_k + \lambda_6\ddot{\mathbf{q}}_k) \tag{16}$$

where:

$$\begin{aligned} &\lambda_1 = \frac{1}{\beta\Delta t^2};\ \lambda_2 = \frac{1}{\beta\Delta t};\lambda_3 = \frac{1}{2\beta} - 1; \\ &\lambda_4 = \frac{\alpha}{\beta\Delta t};\lambda_5 = \frac{\alpha}{\beta} - 1;\lambda_6 = \left(\frac{1}{2\beta} - 1\right)\Delta t \end{aligned} \tag{17}$$

In conclusion, based on the displacement q, the velocity $\dot{q}$, the acceleration $\ddot{q}$ at time k, and the external force at time $k+1$, the displacement q, velocity $\dot{q}$, and acceleration $\ddot{q}$ at time $k+1$ can be obtained. The initial configuration of the drillstring is known, and the motion state at any time can be derived from the initial configuration.

4.1.2. Improved Newton-Raphson Method

After discretizing the control equation in the time domain using the Newmark method, in order to ensure the convergence of the solution for the drillstring dynamics equation, the improved Newton-Raphson method is used to iteratively calculate the approximate solutions obtained by Newmark for each time step. The final iterative value obtained at each time is taken as the exact solution at that time. Unlike the conventional Newmark method, in which iterations are performed at each time step until a convergence criterion is satisfied, the improved Newton–Raphson algorithm prescribes a fixed number of iterations N (for the Newmark integrator, N=3 is found to be optimal). After completing N iterations, the current solution is accepted regardless of the residual magnitude, and the procedure proceeds to the next time step. In addition, within each time step, the Jacobian matrix is fixed: it is computed only once during the first iteration, and subsequently reused in the remaining iterations. This avoids repeated assembly and factorization of the matrix. Since in nonlinear dynamic problems the tangent stiffness typically does not change significantly between successive iterations, employing a fixed Jacobian is sufficient to drive convergence while achieving a significant improvement in computational efficiency. According to Equation (41), the residual stress (residual) R_{k+1} can be expressed as:

$$\mathbf{R}_{k+1} = (\lambda_1\mathbf{M} + \lambda_4\mathbf{C} + \mathbf{K})\mathbf{q}_{k+1} - \mathbf{F}_{k+1} - M(\lambda_1\mathbf{q}_k + \lambda_2\dot{\mathbf{q}}_k + \lambda_3\ddot{\mathbf{q}}_k) - \mathbf{C}(\lambda_4\mathbf{q}_k + \lambda_5\dot{\mathbf{q}}_k + \lambda_6\ddot{\mathbf{q}}_k) \tag{18}$$

Combining Equations (12) and (13), performing a Taylor expansion on the displacement expression of the residual force expression (18) at the j-th iteration of the *k+1*th time step and ignoring the higher-order expansion terms, the iterative expression of the displacement response of the drillstring system is:

$$\mathbf{q}_{k+1}^{(j+1)} = \mathbf{q}_{k+1}^{(j)} - [\mathbf{J}_{k+1}^{(j)}]^{-1}\mathbf{R}_{k+1}^{(j)} \tag{19}$$

where, $J_{k+1}^{(j)}$ represents the Jacobian matrix at the *k+1*th time step and the j-th iteration, which can be expressed as

$$\mathbf{J}_{k+1}^{(j)} = \left.\frac{\partial \mathbf{R}}{\partial \mathbf{q}}\right|_{q_{k+1}^j} = \lambda_1\mathbf{M} + \lambda_4\mathbf{C} + \left.\frac{\partial(\mathbf{Kq} - \mathbf{F})}{\partial q}\right|_{q_{k+1}^j} \tag{20}$$

Since in each time-step iteration, only the complete Jacobian matrix is calculated in the first iteration, and this matrix is reused in subsequent iterations, therefore $J_{k+1}^{(j)}$ can be expressed as:

$$\mathbf{J}_{k+1}{}^{(j)} = \mathbf{J}_{k+1}{}^{1}(j > 1) \tag{21}$$

ISSN: 2688-8645

To solve the dynamic equations of the drill string system, the formulas from (11) to (21) need to be recalculated. The iteration should be terminated early if the displacement convergence criterion is met.

$$\left\|\mathbf{q}_{k+1}^{(j+1)}-\mathbf{q}_{k+1}^{(j)}\right\| \leq \varepsilon^{'}\left\|\mathbf{q}_{k+1}^{(j+1)}\right\| \tag{22}$$

where, $\varepsilon^{'}$ represents the convergence tolerance, $\varepsilon^{'}$=0.00001.

5. Dynamic Response of the Drillstring–Bit Coupled System

The wellbore trajectory of the drilling column system simulation model in this paper is shown in figure 5. The drillstring system consists of 165 drill pipes, 32 weighted drill pipes, 20 drill collars, one stabilizer and one bit. In the built-up and the horizontal sections, the contacts between the drill pipe and the wellbore wall is mainly caused by the gravity of the drill pipe. Therefore, the drill pipe in the built-up section and the horizontal section is modeled using beam elements with a length of 4 meters. The drill pipe in the vertical section is modeled using beam elements with a length of 10 meters.

Table 1. Basic parameters of drillstring and rock

parameter	unit	value	parameter	unit	value
Lenth of dril bit	m	2	Outer diameter of bit	mm	165
Lenth of dril pipe	m	1650	Outer diameter of drill pipe	mm	101
Lenth of drill collar	m	200	Outer diameter of HWDP	mm	101
Length of HWDP	m	320	Outer diameter of drill collar	mm	121
Length of stabilizer	m	3	Outer diameter of stabilizer	mm	160
Density of drill pipe	kg/m^3	7850	Inner diameter of drill pipe	mm	82
Density of drill collar	kg/m^3	7850	Inner diameter of HWDP	mm	65
Density of Drilling fluid	kg/m^3	1200	Inner diameter of drill collar	mm	57
Young's modulus	Pa	210×10^8	Poisson ratio	-	0.3
Eccentric distance	mm	3	Stiffness of the contact	N/m	2×10^8
Static friction coefficient	-	0.3	Kinetic friction coefficient	-	0.2

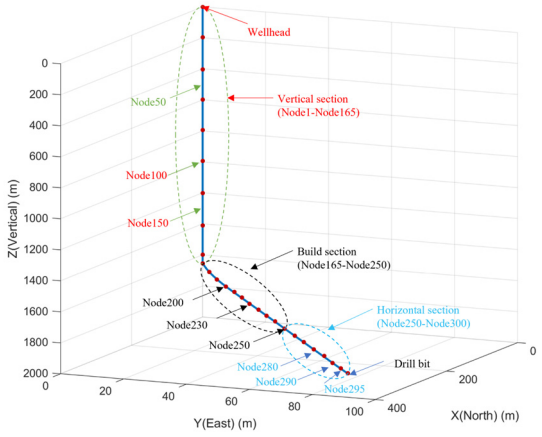

Fig 5. Wellbore trajectory under the global coordinate system

ISSN: 2688-8645

5.1. Drillstring Dynamics Analysis

5.1.1. Study on the Turbulent Trajectory of Drillstring

Maintaining the WOB at 40kN, the vortex trajectories of the drillstring under different rotating speeds are shown in Figure 6. In the vertical well section (node 100), the lateral displacement of the drillstring is relatively small, and the elliptical motion trajectory is stable. Therefore, the main research object is the lateral displacement of the drillstring in the declination section (node 200, node 250) and the horizontal section (node 280). As can be seen from Figures (b)-(c), when the rotating speed is 30 r/min, due to the relatively low applied rotating speed, the drillstring is significantly affected by gravity, and the lateral displacement is small. The drillstring in the built-up section and the horizontal section all stabilize at the lower edge of the wellbore after a brief vortex movement. This indicates that when the rotational speed is low, the movement of the drill string is relatively stable. When the rotating speed is 60 r/min, the range of upward movement of each node expands further, and the drillstring near node 280 begins to contact the upper edge of the wellbore, but the drillstring still moves mainly in the lower right corner of the wellbore. This is because as the rotating speed gradually increases, the centrifugal force and frictional force acting on the drillstring increase, and the drillstring gradually jumps away from the lower edge of the wellbore and begins to contact the upper edge of the wellbore.

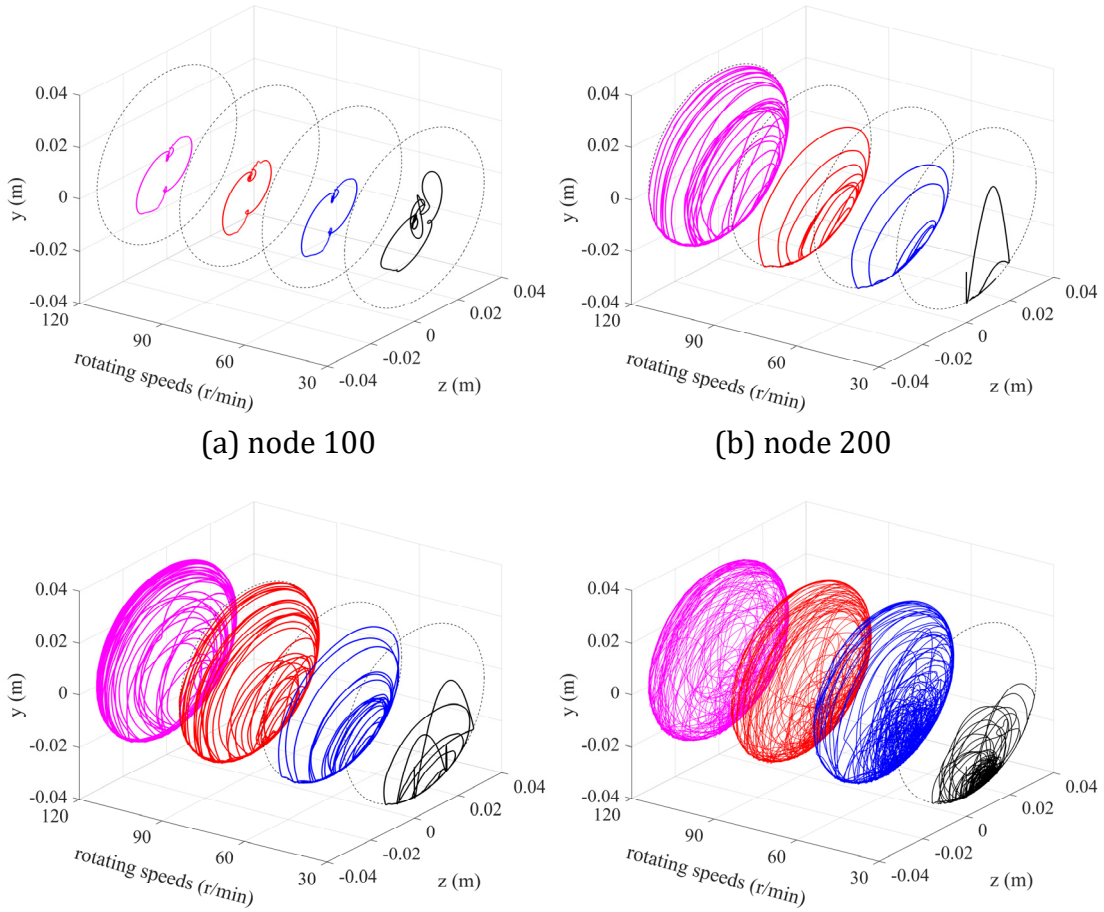

(a) node 100 (b) node 200

(c) node 250 (d) node 280

Fig 6. Trajectory diagrams of vortex motion in the inclination-making section under different rotating speeds

This indicates that increasing the rotational speed will enhance the vortex effect of the drill string. At this point, although there is some vibration in the drill string as the speed increases,

ISSN: 2688-8645

it remains within the acceptable range. Until the rotating speed is increased to 120 r/min, the vortex trajectories of the drillstring around the entire wellbore are filled, and the drillstring frequently collides with the wellbore wall, and the movement trajectory of the node near the bit (node 280) is complex and irregular. This indicates that excessively high rotational speed will cause the drill string to malfunction. Thus, it can be seen that the lateral vortex intensity of the drill string gradually increases with the increase in rotational speed, and it becomes more pronounced the closer it is to the drill bit position. This law reveals the critical relationship between rotational speed and lateral stability: excessively high rotational speed leads to frequent collisions with the well wall, not only intensifying local wear but also possibly causing wellbore instability and drill bit eccentric wear. Therefore, from an engineering application perspective, when the wellbore stability is poor, the rotational speed should be controlled below 60 r/min to avoid the system entering the strong nonlinear vibration zone.

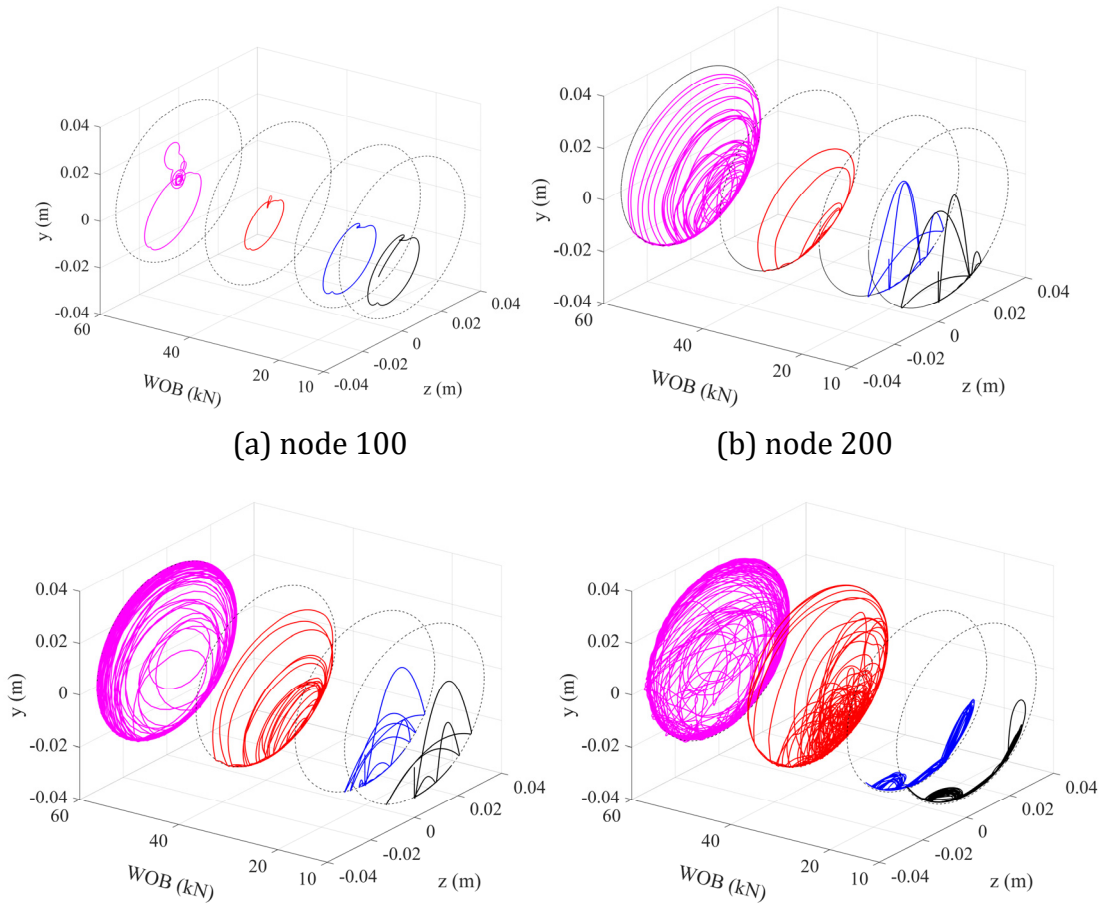

(a) node 100 (b) node 200

(c) node 250 (d) node 280

Fig 7. Trajectory diagram of vortex motion in the inclined section under different WOBs

Maintaining the rotating speed at 60 r/min, the trajectory diagrams of the drillstring's vortex motion under different WOB are shown in figure 7. When the WOB is relatively low (WOB = 10kN and WOB = 20kN), the lateral displacement of the drillstring near the three nodes is small, and the movement state is stable. After a brief jump, it concentrates on the lower side of the wellbore for low-frequency vibration. As the WOB gradually increases, the lateral displacement of the drillstring increases, and it begins to deviate from the lower side. When the WOB is 40kN, the vortex motion range near nodes 200 and 250 of the drillstring expands, and the drillstring near node 280 begins to contact the upper side of the wellbore but the vortex trajectory still concentrates on the lower side of the wellbore. When the WOB is increased to 60kN, the

ISSN: 2688-8645

drillstring near the three nodes contacts the upper side of the wellbore frequently, and the vortex trajectory covers the wellbore. The vortex trajectory near the node close to the bit presents a chaotic state, which is due to the drill string undergoes significant lateral deformation under high drilling pressure, and the vortex phenomenon is extremely intense. In conclusion, excessively high drilling pressure will cause intense vortex effects in the drill string, resulting in frequent wellbore collisions and potential fatigue damage. From an engineering perspective, when the wellbore stability is poor, the drilling pressure should be controlled below 40 kN to avoid the system entering the nonlinear instability zone.

5.1.2. Lateral Acceleration

Maintaining the WOB at 40kN, the variations of the lateral acceleration and its root mean square (RMS) values of the drillstring nodes under different rotary speeds are shown in Fig. 8. At low rotating speeds (30r/min), the amplitudes of the lateral accelerations at the three nodes are all below 5g, indicating that the drillstring is moving stably at this time and has not collided with the wellbore wall. This is consistent with the previous results of the vortex trajectory of the drillstring. As the rotating speed increases, the collisions between the drillstring and the wellbore wall become more frequent, and the normal contact force and tangential friction force also increase. The amplitudes of the lateral accelerations in the y and z directions at each node increase significantly. Especially when the rotating speed reaches 120r/min, the amplitude of the lateral acceleration in the y direction at node 280 reaches 30g, which has a very significant impact on the service life of the bit.

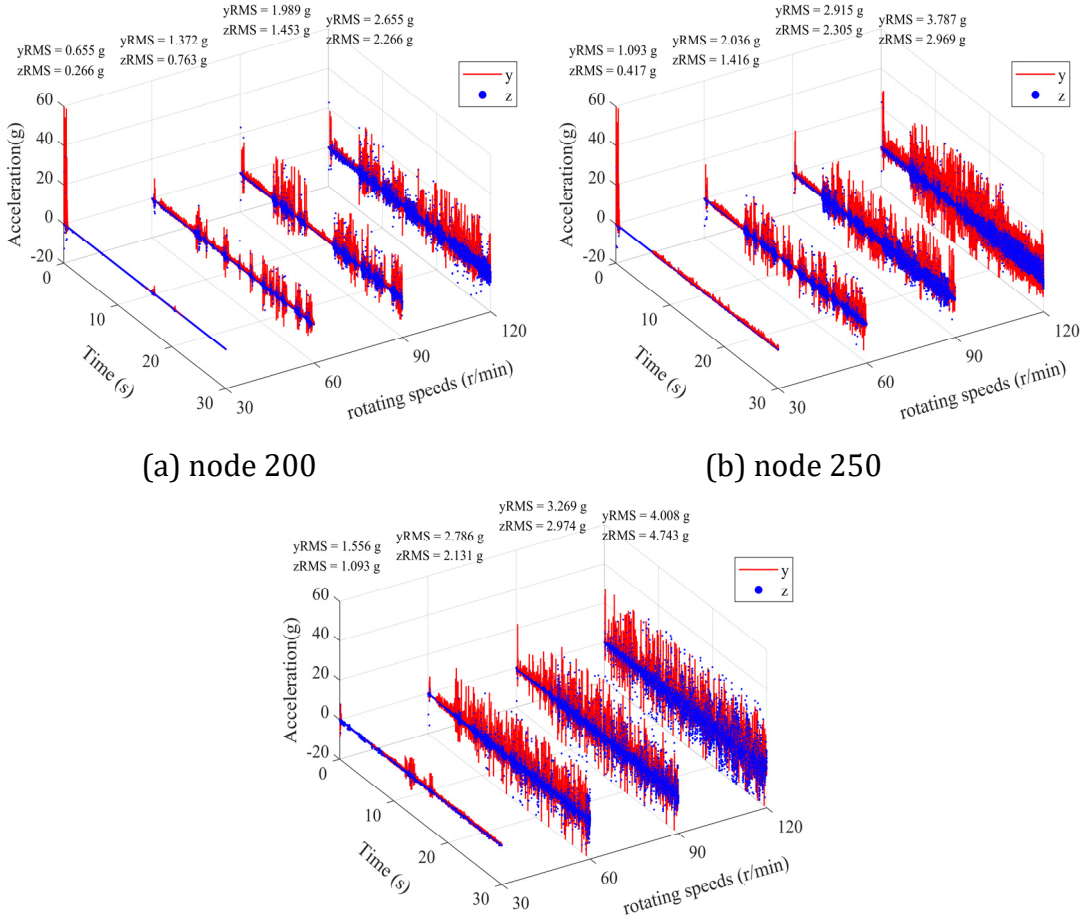

(a) node 200 (b) node 250

(c) node 280

Fig 8. Lateral acceleration and its RMS values diagram of the build-up section under different rotating speeds

ISSN: 2688-8645

This trend can also be observed from the acceleration RMS values of different nodes under various rotary speeds. As the rotary speed increases, the acceleration RMS values in the y- and z-directions of all nodes show an upward trend, indicating that the lateral vibration intensity of the drillstring increases with speed. It is worth noting that the slope changes of the piecewise curves for the y- and z-direction acceleration RMS values at node 280 are larger than those at nodes 200 and 250.This indicates that, compared with nodes 200 and 250, the increase in rotating speed has a more significant impact on the lateral acceleration of node 280. This is because node 280 is close to the bit, and the gap between the drillstring and the wellbore at this location is smaller. Once the rotating speed increases, collisions with other nodes are more frequent, so the lateral acceleration change at node 280 is more obvious. To increase the service life of the drillstring and reduce lateral vibration, the driving rotating speed should be set between 30 and 60r/min.

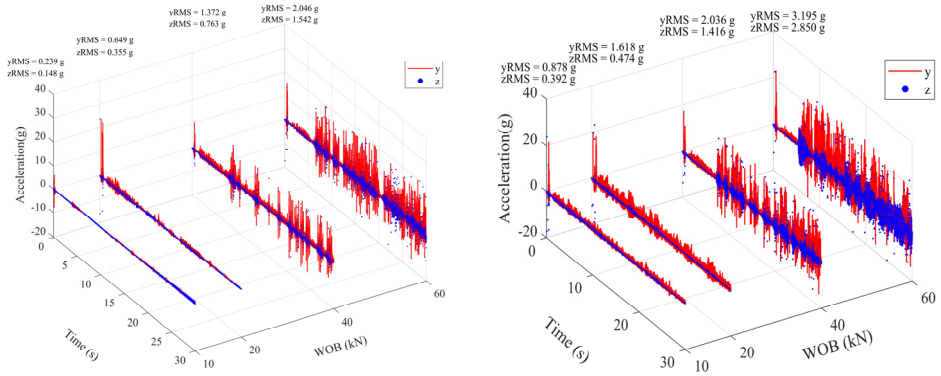

(a) node 200 (b) node 250

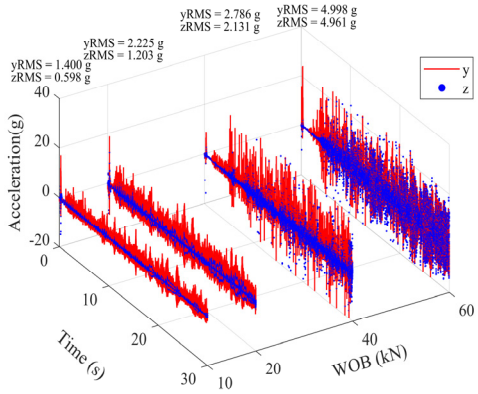

(c) node 280

Fig 9. Lateral acceleration and its RMS values diagram of the build-up section under different WOBs

Maintaining the rotating speed at 60r/min, the lateral acceleration and its RMS values of the drillstring nodes under different WOB is shown in Figure 9. The influence of WOB on the lateral acceleration of the drillstring is similar to that of rotary speed: under the same WOB, the closer the node is to the bit, the higher the frequency and amplitude of lateral vibration, and the larger the RMS values of acceleration in the y- and z-directions. This is because the smaller annular clearance between the drillstring and the borehole results in more significant changes in vibration frequency and amplitude. As WOB increases, the vibration frequency, amplitude, and RMS values in the y- and z-directions of the same node also increase. When WOB reaches 60 kN, the lateral acceleration of the drillstring is as high as 30g, which adversely affects bit service

ISSN: 2688-8645

life. However, the mechanisms of vibration changes induced by WOB and rotary speed differ: with higher WOB or at positions closer to the bit, the drillstring is more prone to bending deformation, which leads to severe impacts. Therefore, WOB should be maintained below 40 kN.

5.2. Bit Dynamics Analysis

5.2.1. Dynamic Response of the Bit under Different Rotating Speeds

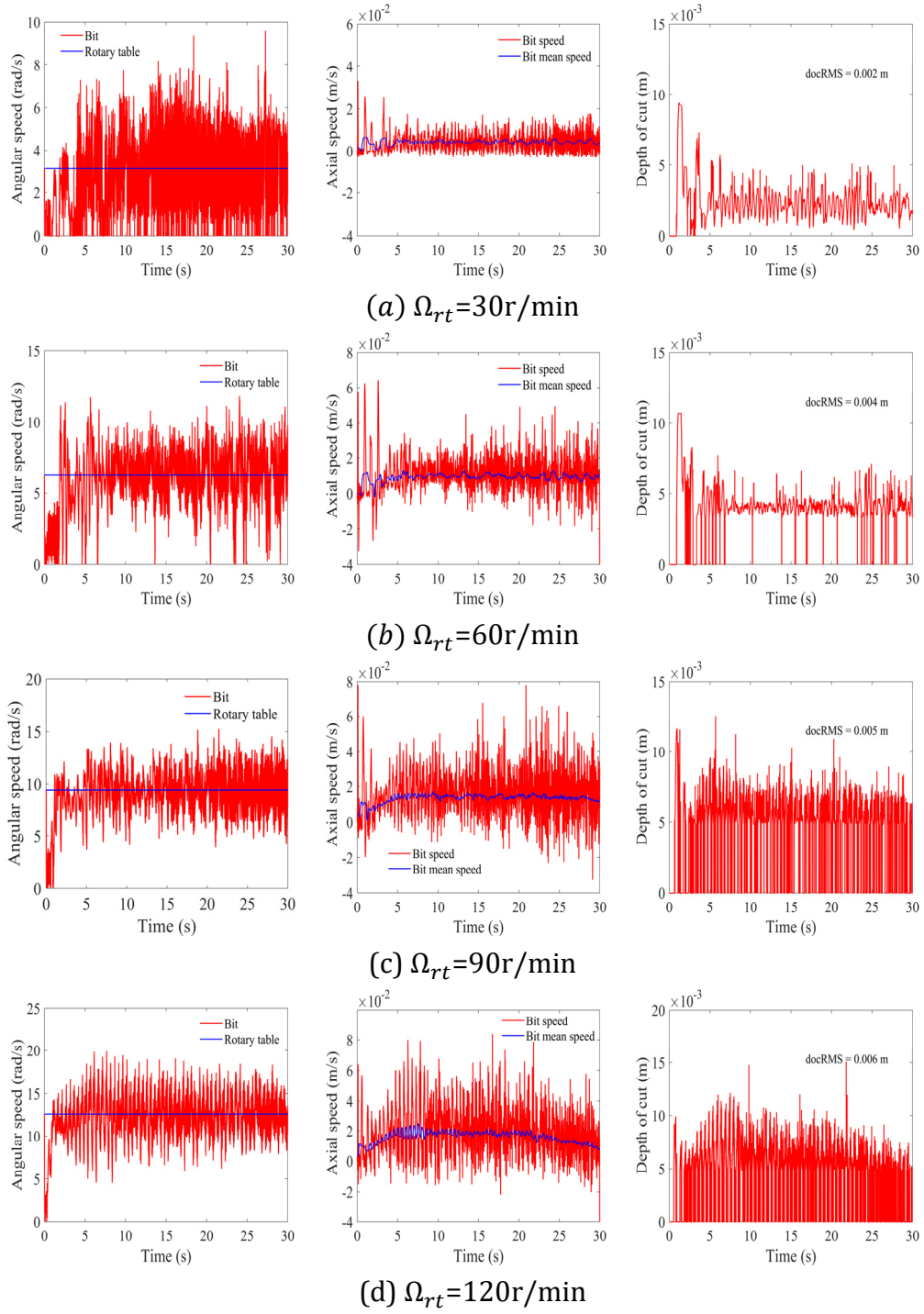

(a) Ω_{rt}=30r/min

(b) Ω_{rt}=60r/min

(c) Ω_{rt}=90r/min

(d) Ω_{rt}=120r/min

Fig 10. Dynamic response of the bit under different rotating speeds

Maintaining the WOB at 40kN, the angular velocity, axial velocity and cutting depth of the bit under different rotating speeds are shown in Figure 10. From the angular velocity graph and axial velocity graph of the bit, it can be seen that when the rotating speed is low (30r/min), the

ISSN: 2688-8645

bit exhibits stick-slip phenomena in both the torsional and axial directions (angular velocity or axial velocity is 0). As the rotary table speed increases, the stick-slip effect gradually weakens. When the rotating speed is 60 r/min, the axial stick-slip effect disappears, while the torsional stick-slip effect still exists. Until the rotating speed increases to 90r/min and 120r/min, both stick-slip effects completely disappear. Analyzing the time-domain variation graph of the cutting depth of the bit, when the rotating speed is 60r/min, the sticking phenomenon (cutting depth is 0, axial velocity is less than 0) begins to occur. Especially when the rotating speed is large (90r/min and 120r/min), the sticking phenomenon occurs frequently, seriously affecting the service life of the bit. From the cutting depth graphs in Figures (a)-(d), it can be seen that the amplitude of axial velocity and cutting depth increase positively with the increase of rotating speed. When the rotational speed is 120 r/min, the amplitude of the axial velocity is 0.08 m/s, the amplitude of the cutting depth is 0.012 m, and the RMS value is 0.006m. All of these exceed those at other rotational speeds. This indicates that increasing the rotary speed can improve the rate of penetration (ROP). In conclusion, increasing the rotating speed can effectively reduce the stick-slip effect during cutting and increase the feed speed of the bit, but a large rotating speed will lead to an intensified sticking effect of the bit. Therefore, a rotary speed of 60 r/min is recommended.

5.2.2. Dynamic Response of the Bit under Different WOB

Maintaining the rotating speed at 60r/min, the angular velocity, axial velocity and cutting depth of the bit under different WOB are shown in Figure 11. From the angular velocity graph and axial velocity graph of the bit, it can be seen that the axial frictional sliding effect occurs under the low WOB (10kN) condition, while the torsional direction's frictional sliding effect occurs under the high WOB (40kN and 60kN) conditions. This is because the torsional direction's frictional sliding effect is mainly caused by the frictional torque, and the larger the WOB, the greater the frictional torque, and the more obvious the influence on the torsional direction's frictional sliding effect; while the axial frictional sliding effect is mainly caused by the axial frictional resistance, and the larger the WOB, the axial frictional resistance remains unchanged, and the influence of the axial frictional resistance on the motion becomes smaller and smaller. Combining the time-domain change graph of the bit's cutting depth, it can be seen that at low WOB, the bit does not exhibit a skipping drill phenomenon. When the WOB increases to 40 kN, the skipping drill phenomenon begins to occur and becomes more frequent as the WOB increases. From the amplitude of the axial velocity graph and the cutting depth graph, it can be seen that as the WOB increases, the amplitude of the axial velocity and the cutting depth both increase: the maximum of the axial average velocity and the cutting depth from low pressure of 10kN is 10×10^{-3} m/s and 6×10^{-3} m respectively, increases to 7×10^{-2} m/s and 16×10^{-3} m at high pressure of 60kN. This indicates that increasing the drilling pressure can also enhance the ROP of the drill bit. However, compared with the influence of rotational speed on the ROP of the drill bit, the impact of WOB on the axial speed and cutting depth of the drill bit is more significant, that is, the amplitude change is more obvious. This suggests that increasing the drilling pressure can more effectively improve the feed efficiency of the drill bit. However, when the WOB is higher than 40kN, the amplitude change weakens, which is due to the intensification of the torsional direction's frictional sliding effect, affecting the feed of the bit. In conclusion, increasing the WOB is beneficial to improving the drilling efficiency and reducing the axial frictional sliding effect, but an excessively high WOB will intensify the torsional direction's frictional sliding effect and reduce the life of the bit. Therefore, a weight on bit (WOB) of 40 kN is recommended.

ISSN: 2688-8645

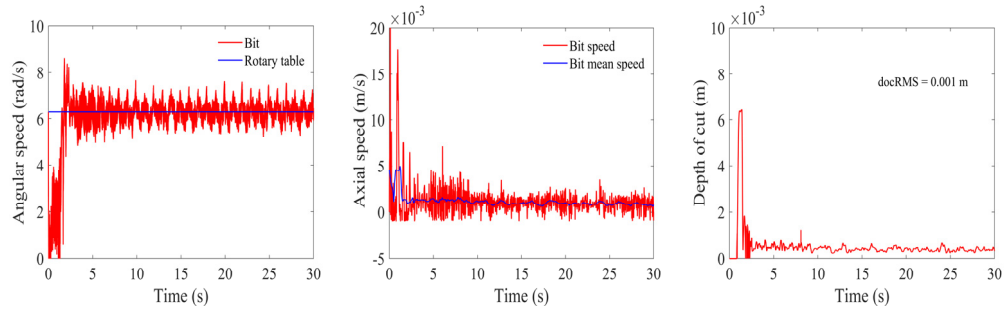

(a) WOB=10kN

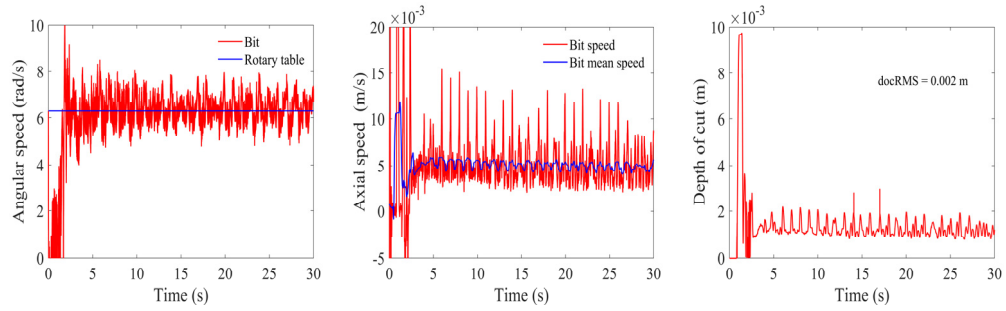

(b) WOB=20kN

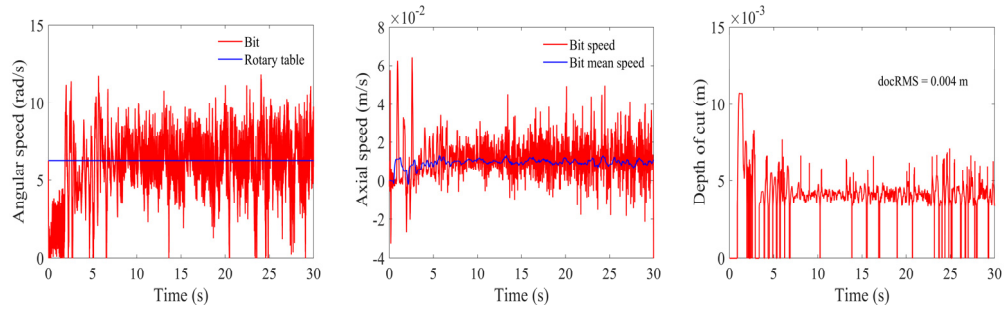

(c) WOB=40kN

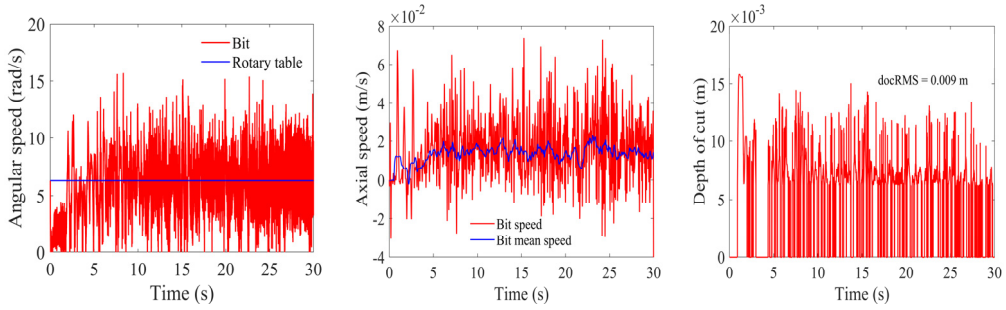

(d) WOB=60kN

Fig 11. Dynamic response of the bit under different WOBs

6. Conclusion

This paper focuses on the study of the downhole dynamics of horizontal wells. Under the premise of fully considering the three-dimensional curved wellbore trajectory and the complex external force conditions in the well, the finite element method is used to establish a mathematical model of the drill string system equipped with a circular cutting tooth PDC drill bit. At the same time, a drill bit-rock interaction model that can fully consider the geometric parameters and state delay-dependent effects of the drill bit as well as the multiple cutting effects is established using polygon clipping technology and projection principles. Finally,

ISSN: 2688-8645

through numerical solution of the coupled model of drill string - drill bit - rock, the following conclusions are drawn:

(1) The WOB and rotary speed have a significant impact on the dynamic behavior of the drillstring. For the build-up section of the drillstring (nodes 200 and 250) and the horizontal section (node 280), both higher weight on bit (40 kN) and higher rotary speed (60 r/min) intensify the whirl phenomenon of the drillstring, though the underlying mechanisms differ. Excessive weight on bit (60 kN) and high rotary speed (120 r/min) cause frequent collisions between the drillstring near the bit in the horizontal section (node 280) and the borehole wall, which leads to severe wear of the drillstring and may hinder normal drilling operations. Therefore, when only considering the drill string section, the recommended drilling pressure is below 40 kN, and the recommended rotational speed is between 30 and 60 r/min.In addition, an increase in the local curvature of the wellbore trajectory in the build-up section enhances the whirl motion and vibration intensity of the drillstring in that region. Therefore, the wellbore trajectory should be reasonably designed based on drillstring dynamic simulation results.

(2) The drilling parameters and rock properties have a noticeable influence on the dynamic response of the drill bit. Under a higher weight on bit (60 kN), the bit exhibits stick–slip in the torsional direction and bit bounce in the axial direction, leading to severe axial and torsional vibrations that shorten bit service life. Reducing the weight on bit can effectively mitigate stick–slip and bit bounce; however, it may cause axial stick–slip. At a high rotary speed (120 r/min), the stick–slip phenomenon disappears while bit bounce becomes more evident, whereas at a low rotary speed, stick–slip is dominant and bit bounce is weakened. Nevertheless, appropriately increasing both weight on bit and rotary speed can improve drilling efficiency and increase the ROP. In summary, a weight on bit of 40 kN and a rotary speed of 60 r/min are recommended, as the drillstring whirl remains stable and the bit vibration intensity and ROP are moderate under these conditions. Moreover, higher intrinsic specific energy and contact pressure of the rock lead to stronger bit vibrations, with the axial vibration being more sensitive. Therefore, when drilling in harder formations, the weight on bit and rotary speed should be appropriately reduced.

(3) This study provides a theoretical basis for the optimization of drilling parameters, bit selection, and bottom-hole assembly design, which can effectively suppress the vibration of the drillstring system, improve drilling efficiency, and extend the service life of both the drillstring and the bit. Based on this model, a coupled dynamic model between the drillstring and drilling fluid can be developed in the future to analyze the influence of drilling fluid on the dynamic behavior of the drillstring system. Additionally, the model can be extended to the downhole dynamic analysis of power drilling tools such as mud motors.

Declarations

Conflict of Interest The authors declare that they have no known competing financial interests or personal relationships that could have appeared to influence the work reported in this paper.

Abbreviations

BHA	Bottom hole assembly
WOB	Weight on bit
SDD	State-dependent delay
RMS	Root Mean Square
ROP	Rate of penetration

ISSN: 2688-8645

References

[1] Li, W., Huang, G., Jing, Y., Yu, F., & Ni, H. (2019). Modeling and mechanism analyzing of casing running with pick-up and release technique. Journal of Petroleum Science and Engineering, 172, 538-546. https://doi.org/10.1016/j.petrol.2018.09.099.

[2] Jianhong, F., Kexiong, S., Zhi, Z., Dezhi, Z., Fei, L., Xin, X., & Xin, Z. (2012). Stress analysis on drilling string vibration in gas drilling. Energy Procedia, 16, 1264-1268. https://doi.org/ 10.1016/ j.egypro. 2012. 01.202.

[3] Song, J., Liu, S., He, Y., Jiang, S., Zhou, S., & Zhu, H. (2024). The state-of-the-art review on the drill pipe vibration. Geoenergy Science and Engineering, 243, 213337. https://doi.org/ 10.1016/ j.geoen. 2024. 213337.

[4] Aarsnes, U. J. F., & Van De Wouw, N. (2018). Dynamics of a distributed drill string system: Characteristic parameters and stability maps. Journal of Sound and Vibration,417, 376-412. https://doi.org/10.1016/j.jsv.2017.12.002.

[5] Moharrami, M. J., de Arruda Martins, C., & Shiri, H. (2021). Nonlinear integrated dynamic analysis of drill strings under stick-slip vibration. Applied Ocean Research,108, 102521. https:// doi. org/ 10. 1016/ j.apor.2020.102521.

[6] Xie, D., Wu, Q., Xi, Y., & Huang, Z. (2023). Global modelling of nonlinear spatiotemporal dynamics of a drill-string with multiple regenerative effects. Applied Mathematical Modelling,114, 114-132. https:// doi.org/10.1016/j.apm.2022.09.037.

[7] Han, C.J., Yan, T., Bi, X.L., et al., 2005. Analysis on drill string vibration of deep wells. Natural Gas Industry, 25 (9), 76–79.https://doi.org/10.3321/j.issn:1000-0976.2005.09.025.

[8] Li, Z., Zhang, C., & Song, G. (2017). Research advances and debates on tubular mechanics in oil and gas wells. Journal of petroleum science and engineering, 151, 194-212. https://doi.org/ 10. 1016/ j.petrol. 2016.10.025.

[9] Ren, F., Chen, S., & Yao, Z. (2013). Vibration response analysis of slender flexible revolving beam under axial load. China Mechanical Engineering, 24(24), 3392. https://doi.org/10. 3969/ j. issn. 1004-132X.2013.24.025.

[10] Meng, Q.H., Liu, Q.Y., 2011. Establishment of gas-solid coupled transverse vibration mathematical model of drilling string in gas drilling and its control. Mathematics in Practice and Theory 41 (13), 88–93. https://link.cnki.net/doi/CNKI:SUN:SSJS.0.2011-13-014.

[11] Fan, H.H., Yang, X., Wang, Y., et al., 2015. Analysis on lateral vibration features of production string in high pressure gas wells. China Petroleum Machinery 43 (3), 88–91+95. https://doi. org/10. 16082/ j. cnki.issn.1001-4578.2015.03.019.

[12] Gupta, S. K., & Wahi, P. (2016). Global axial–torsional dynamics during rotary drilling. Journal of Sound and Vibration, 375, 332-352. https://doi.org/10.1016/j.jsv.2016.04.021.

[13] Yigit AS, Christoforou AP. Stick-Slip and Bit-Bounce Interaction in Oil-Well Drillstrings[J]. Journal of Energy Resources Technology-transactions of The Asme, 2006, 128: 268-274. https://doi. org/ 10.1115/1.2358141.

[14] Wang, B., Wang, Z., & Ren, F. (2020). Dynamic Model and Quantitative Analysis of Stick-Slip Vibration in Horizontal Well. Shock and Vibration, 2020(1), 8831111. https://doi.org/ 10.1155/ 2020/ 8831111.

[15] Cai, M., Mao, L., Xing, X., Zhang, H., & Li, J. (2022). Analysis on the nonlinear lateral vibration of drillstring in curved wells with beam finite element. Communications in Nonlinear Science and Numerical Simulation, 104, 106065. https://doi.org/10.1016/j.cnsns.2021.106065.

[16] Tobias, S. A. (1961). Machine tool vibration research. International Journal of Machine Tool Design and Research, 1(1-2), 1-14. https://doi.org/10.1016/0020-7357(61)90040-3.

[17] Liu, X., Vlajic, N., Long, X., Meng, G., & Balachandran, B. (2014). Coupled axial-torsional dynamics in rotary drilling with state-dependent delay: stability and control. Nonlinear Dynamics,78(3), 1891-1906. https://doi.org/10.1007/s11071-014-1567-y.

[18] Zhu, L., Jiang, Z., Shi, J., & Jin, C. (2015). An overview of turn-milling technology.The International Journal of Advanced Manufacturing Technology, 81(1), 493-505. https://doi.org/10.1007/s00170-015-7187-y.

[19] Caixu, Y. U. E., Haining, G. A. O., Xianli, L. I. U., Steven, Y. L., & Lihui, W. A. N. G. (2019). A review of chatter vibration research in milling. Chinese Journal of Aeronautics, 32(2), 215-242. https:// doi. org/ 10.1016/j.cja.2018.11.007.

[20] Detournay, E., & Defourny, P. (1992, January). A phenomenological model for the drilling action of drag bits. In International journal of rock mechanics and mining sciences & geomechanics abstracts(Vol. 29, No. 1, pp. 13-23). Pergamon. https://doi.org/10.1016/0148-9062(92)91041-3.

[21] Tian, K., & Detournay, E. (2021). Influence of PDC bit cutter layout on stick–slip vibrations of deep drilling systems. Journal of Petroleum Science and Engineering, 206, 109005. https://doi. org/ 10.1016/j.petrol.2021.109005.

[22] Rubey, W. W., & King Hubbert, M. (1959). Role of fluid pressure in mechanics of overthrust faulting: II. Overthrust belt in geosynclinal area of western Wyoming in light of fluid-pressure hypothesis. Geological Society of America Bulletin, 70(2), 167-206. https://doi.org/10.1130/0016-7606 (1959) 70 [167:ROFPIM]2.0.CO;2.

[23] Qinfeng, D. I., Mingming, Y. O. U., Tianxin, L. I., Xing, Z. H. O. U., Heyuan, Y. A. N. G., & Wenchang, W. A. N. G. (2024). Simulation and analysis of dynamic characteristics of drilling string in extra-deep wells. Petroleum Drilling Techniques, 52(2), 108-117. http://dx.doi.org/10.11911/syztjs.2024029.

[24] Zhao, D., Hovda, S., & Sangesland, S. (2016, June). The effect of stick slip vibration on the backward whirl of bottom hole assembly in drillstring. In International Conference on Offshore Mechanics and Arctic Engineering (Vol. 49996, p. V008T11A042). American Society of Mechanical Engineers. https://doi.org/10.1115/0MAE2016-54478.

[25] Xu, J., Huang, Y., & Qu, Z. (2020). An efficient and unconditionally stable numerical algorithm for nonlinear structural dynamics. International Journal for Numerical Methods in Engineering, 121 (20), 4614-4629. https://doi.org/10.1002/nme.6456.